10.1098/rsta.2003.1337

THE ROYAL SOCIETY

A fast multipole method for Maxwell equations stable at all frequencies

By Eric Darve[1] and Pascal Havé[2]

[1]*Mechanical Engineering Department, Stanford University, Stanford, CA 94305-4040, USA* (darve@stanford.edu)
[2]*Laboratoire Jacques-Louis Lions, Université Pierre et Marie Curie, Boîte courrier 187, 75252 Paris Cedex 05, France* (have@ann.jussieu.fr)

Published online 29 January 2004

The solution of Helmholtz and Maxwell equations by integral formulations (kernel in $\exp(\mathrm{i}kr)/r$) leads to large dense linear systems. Using direct solvers requires large computational costs in $O(N^3)$. Using iterative solvers, the computational cost is reduced to large matrix–vector products. The fast multipole method provides a fast numerical way to compute convolution integrals. Its application to Maxwell and Helmholtz equations was initiated by Rokhlin, based on a multipole expansion of the interaction kernel. A second version, proposed by Chew, is based on a plane-wave expansion of the kernel.

We propose a third approach, the stable-plane-wave expansion, which has a lower computational expense than the multipole expansion and does not have the accuracy and stability problems of the plane-wave expansion. The computational complexity is $N \log N$ as with the other methods.

Keywords: fast multipole method; integral equations; electromagnetics; scattering; radar cross-section; singular value decomposition

1. Introduction

(*a*) *Multipole expansion*

The basic problem that the fast multipole method (FMM) addresses is that of computing large matrix–vector products, where the matrix is defined by

$$M_{ij} = \frac{\exp(\mathrm{i}\kappa|\boldsymbol{r}_i - \boldsymbol{r}_j|)}{|\boldsymbol{r}_i - \boldsymbol{r}_j|}.$$

The FMM of Greengard *et al.* (1998) is based on the following multipole expansion:

$$h_0^{(1)}(\boldsymbol{r} + \boldsymbol{r}') = \sum_{n=0}^{+\infty} (-1)^n (2n+1) h_n^{(1)}(\kappa|\boldsymbol{r}|) j_n(\kappa|\boldsymbol{r}'|) P_n(\boldsymbol{r} \cdot \boldsymbol{r}'), \tag{1.1}$$

where $h_n^{(1)}$ is the spherical Hankel function, j_n the spherical Bessel function and P_n the Legendre polynomial. As the FMM has been described in more detail elsewhere

One contribution of 13 to a Theme 'Short-wave scattering'.

(Epton & Dembart 1995; Dembart & Yip 1994, 1995; Dembart & Shubin 1994), we will only summarize the key formulae here so that the notation is clarified. Two fundamental solutions can be defined, one which is regular, the other singular at $\boldsymbol{r} = \mathbf{0}$:

$$I_n^m(\boldsymbol{r}) = \mathrm{i}^n j_n(\kappa|\boldsymbol{r}|)L_n^m(\theta,\phi),$$
$$O_n^m(\boldsymbol{r}) = \mathrm{i}^n h_n^{(1)}(\kappa|\boldsymbol{r}|)N_n^m(\theta,\phi),$$

where L_n^m and N_n^m are equal to spherical harmonics up to the choice of normalizing constants:

$$L_n^m(\theta,\phi) = \frac{\sqrt{2n+1}}{(n+|m|)!}P_n^m(\cos\theta)\mathrm{e}^{-\mathrm{i}m\phi},$$
$$N_n^m(\theta,\phi) = \sqrt{2n+1}(n-|m|)!P_n^m(\cos\theta)\mathrm{e}^{\mathrm{i}m\phi}.$$

P_n^m are the associated Legendre functions.

With these choices the formulae are somewhat simplified. Equation (1.1) becomes

$$h_0^{(1)}(\boldsymbol{r}+\boldsymbol{r}') = \sum_{n=0}^{+\infty}\sum_{m=-n,\ldots,n} I_n^m(\boldsymbol{r})O_n^m(\boldsymbol{r}'). \tag{1.2}$$

The usual transforms (inner-to-inner, outer-to-outer, outer-to-inner) are defined in terms of the function E, which is related to the Wigner 3-j symbols or Clebsch–Gordan coefficients (Epton & Dembart 1995)

$$E\begin{pmatrix} m & p & r \\ n & q & s \end{pmatrix} = \frac{1}{4\pi}\iint N_n^m(\theta,\phi)N_q^p(\theta,\phi)L_s^r(\theta,\phi)\sin\theta\,\mathrm{d}\theta\,\mathrm{d}\phi.$$

The outer-to-inner transform then reads

$$O_n^m(\boldsymbol{r}+\boldsymbol{r}') = \sum_{m,n,m',n',s} E\begin{pmatrix} m & m' & m+m' \\ n & n' & n+n'-2s \end{pmatrix} I_{n'}^{m'}(\boldsymbol{r})O_{n+n'-2s}^{m+m'}(\boldsymbol{r}'). \tag{1.3}$$

Similar equations hold for the outer-to-outer and inner-to-inner transforms.

This approach has two disadvantages, which our technique addresses. Firstly, it is not applicable to the high-frequency regime. In fact it can be shown that the number of terms needed in the multipole expansion (the number of terms in (1.1), for example) is of the order of κD, where D is the diameter of the object. As κD becomes large, the method becomes very costly. In the high-frequency regime it is very common that hundreds of terms are needed for the series in (1.1) to start converging. Therefore, it is impractical.

Secondly, the cost of applying the method in the low-frequency regime is still quite high. In fact, the computation of the function E and its multiplication by $O_{n+n'-2s}^{m+m'}(\boldsymbol{r}')$ requires a total of $O(p^5)$ FLOPS (floating point operations per second) for an order-p expansion.

Several publications improve on this original approach. For the Laplace equation, Elliot & Board (1996) reduce the algorithmic complexity by using the fast Fourier transform, and improve stability and efficiency with a block decomposition. Greengard & Rokhlin (1997) introduced two improvements based on rotation matrices (a

method similar to White & Headgordon (1996)) and on a plane-wave expansion, which provides a diagonal multipole-to-local operator. Zhao & Chew (2000*b*) applied a matrix-rotation scheme to reduce the requirement. For the Helmholtz equation, Greengard *et al*. (1998) propose a variant of the scheme described in this article to speed up the multipole-to-local operation.

In order to make this method stable at a very-low-frequency regime, a renormalization of the coefficients is required. Zhao & Chew (1999, 2000*a*) describe this procedure and Zhao & Chew (2001) and Velamparambil & Chew (2001) apply it to low-frequency problems.

An issue which will not be developed in this article is the choice of basis functions for the discrete problem. The usual Rao–Wilton–Glisson basis function is inadequate in the very-low-frequency regime. (See Zhao *et al*. (2002) for a discussion on this topic.)

(*b*) *Plane-wave expansion: high-frequency FMM*

To address the problem of an increased number of multipole terms in the high-frequency regime (Rokhlin 1990, 1992; Lu & Chew 1994; Song *et al*. 1997; Darve 2000*a*,*b*), a different approach, high frequency (HF) FMM, was considered based on the following approximation:

$$\frac{\mathrm{e}^{\mathrm{i}\kappa|\boldsymbol{r}+\boldsymbol{r}'|}}{|\boldsymbol{r}+\boldsymbol{r}'|} = \lim_{p\to+\infty} \int_{S^2} \mathrm{e}^{\mathrm{i}\kappa\langle\sigma,\boldsymbol{r}'\rangle} T_{p,\sigma}(\boldsymbol{r})\,\mathrm{d}\sigma,$$

where S^2 is the unit sphere. We denote by $\langle\cdot,\cdot\rangle$ the scalar product. The function $T_{p,\sigma}(r)$ is defined by

$$T_{p,\sigma}(\boldsymbol{r}) = \mathrm{i}\kappa \sum_{m=0}^{p} \frac{(2m+1)\mathrm{i}^m}{4\pi} h_m^{(1)}(\kappa|\boldsymbol{r}|) P_m(\cos(\sigma,\boldsymbol{r})).$$

The integral is then discretized and an appropriate integer p is chosen so that

$$\frac{\mathrm{e}^{\mathrm{i}\kappa|\boldsymbol{r}+\boldsymbol{r}'|}}{|\boldsymbol{r}+\boldsymbol{r}'|} \approx \sum_k \omega_k \mathrm{e}^{\mathrm{i}\kappa\langle\sigma_k,\boldsymbol{r}'\rangle} T_{p,\sigma}(\boldsymbol{r}). \tag{1.4}$$

Several publications have studied how to appropriately choose the discretization points and the order p for a given accuracy ϵ.

With this approach the cost of the outer-to-inner transform is reduced to $O(p^2)$. This guarantees a computational expense of the order of $N \log N$ in the high-frequency regime.

The transfer function $T_{p,\sigma}(\boldsymbol{r})$ is defined is terms of $h_m^{(1)}(\kappa|\boldsymbol{r}|)$, which has the property of diverging when $m \to +\infty$ or $\kappa|\boldsymbol{r}| \to 0$, i.e. when the size of the clusters becomes very small compared with the wavelength (this problem is known as *sub-wavelength breakdown*).

Coupled to round-off errors, those numerical instabilities lead to a divergence of the method as the number of poles is increased beyond a certain threshold. The method is thus unstable when high accuracy is required or in the low-frequency regime, i.e. when the order p is large.

Despite this limitation, the method has proved to be very successful. Chew has made impressive radar computation using this approach (Chew 1993; Chew *et al*.

1994; Chew & Song 1995; Lu & Chew 1994, 1995; Song *et al.* 1997, 1998*a*, *b*; Wagner & Chew 1994).

Our approach, the stable-plane-wave expansion, solves this problem by being stable from low- to high-frequency regimes and being arbitrarily accurate numerically. The total asymptotic cost is $O(N \log N)$ as for the other methods, and the outer-to-inner transform is performed in $O(p^2)$ FLOPS.

2. Stable-plane-wave expansion

To avoid the stability problem, we follow Greengard *et al.* (1998).

Theorem 2.1.

$$\frac{\mathrm{e}^{\mathrm{i}\kappa|\boldsymbol{r}|}}{|\boldsymbol{r}|} = \frac{\mathrm{i}\kappa}{2\pi}\int_{S^{z+}} \mathrm{e}^{\mathrm{i}\kappa\langle\sigma,\boldsymbol{r}\rangle}\,\mathrm{d}\sigma + \frac{1}{\pi}\int_{\chi=0}^{+\infty}\int_{\phi=0}^{2\pi} \exp\{-\chi^2 z\}\exp\{\mathrm{i}\sqrt{\chi^4+\kappa^2}(x\cos\phi + y\sin\phi)\}\chi\,\mathrm{d}\chi\,\mathrm{d}\phi, \tag{2.1}$$

where

$$S^{z+} = \{\boldsymbol{r} = (x, y, z) \in \mathbb{R}^3,\ |\boldsymbol{r}| = 1,\ z > 0\}$$

(upper hemisphere of the unit sphere).

Even though our approach is based on the same integral, it is, as we will see, different. Compared with Greengard *et al.* (1998), the new approach is applicable to all frequencies, while the previous approach is very costly in high-frequency regimes and uses a single expansion, the stable-plane-wave expansion, rather than a combination of plane-wave expansion and classical multipole expansion.

Hu *et al.* (1999, 2000*a*, *b*, 2001; see also Hu & Chew 2001) proposed a technique (fast inhomogeneous plane-wave algorithm (FIPWA)) based on an integral similar to (2.1). FIPWA and (2.1) are different because the path of the integral in the complex plane is different. FIPWA uses the steepest descent path, whereas (2.1) uses a path parallel to the real or imaginary axis (Hu & Chew 2001).

In order to describe the new approach we need to explain in more detail the basic ingredients of the fast multipole. We will then show how (2.1) can be applied.

(*a*) *Basic requirements of the FMM*

We assume that the reader is familiar with the standard oct-tree decomposition that is classically used for the FMM. We summarize the four basic conditions for constructing an FMM.

Requirement 2.2. *The four basic conditions for constructing an FMM are as follows.*

(1) Multipole expansion. *For any point* $\boldsymbol{r}$ *inside a cluster* C_a *of centre* $\boldsymbol{O}_a$ *and* $\boldsymbol{r}'$ *inside a cluster* C_b *of centre* $\boldsymbol{O}_b$, $n^{\max}$ *functions* $I_q^a(\boldsymbol{r}-\boldsymbol{O}_a)$ *and* $O_q^{ab}(\boldsymbol{O}_a-\boldsymbol{r}')$ *must be defined such that the field* $\exp(\mathrm{i}\kappa|\boldsymbol{r}-\boldsymbol{r}'|)/|\boldsymbol{r}-\boldsymbol{r}'|$ *can be approximated by*

$$\frac{\exp(\mathrm{i}\kappa|\boldsymbol{r}-\boldsymbol{r}'|)}{|\boldsymbol{r}-\boldsymbol{r}'|} \approx \sum_{q=1}^{n^{\max}} \omega_q I_q^a(\boldsymbol{r}-\boldsymbol{O}_a) O_q^{ab}(\boldsymbol{O}_a-\boldsymbol{r}'). \tag{2.2}$$

(2) Outer-to-outer. *For any cluster C_b (of centre $\boldsymbol{O}_b$) which is the child of C_c (of centre $\boldsymbol{O}_c$), a matrix $\bar{I}^{cb}_{pq}$ must be defined such that*

$$I^c_p(\boldsymbol{O}_c - \boldsymbol{r}') \approx \sum_q \bar{I}^{cb}_{pq} I^b_q(\boldsymbol{O}_b - \boldsymbol{r}').$$

(3) Outer-to-inner. *For any two clusters C_a (centre $\boldsymbol{O}_a$) and C_b (centre $\boldsymbol{O}_b$) sufficiently far away, a matrix T^{ab}_{pq} (transfer matrix) must be defined such that*

$$O^{ab}_p(\boldsymbol{O}_a - \boldsymbol{r}') \approx \sum_q T^{ab}_{pq} I^b_q(\boldsymbol{O}_b - \boldsymbol{r}').$$

(4) Inner-to-inner. *For any point $\boldsymbol{r}'$ in cluster C_b and any cluster C_c (centre $\boldsymbol{O}_c$), far away from C_b, and which is the parent of C_a (centre $\boldsymbol{O}_a$), a matrix $\bar{O}^{ac}_{pq}$ must be defined such that*

$$O^{ab}_p(\boldsymbol{O}_a - \boldsymbol{r}') \approx \sum_q \bar{O}^{ac}_{pq} O^{cb}_q(\boldsymbol{O}_c - \boldsymbol{r}').$$

For example, (1.2) can be used to satisfy item (1) and (1.3) can be used for item (3).

The two previous variants of the FMM, the multipole expansion (§ 1 *a*) and plane-wave expansion (§ 1 *b*), provide the functions O^{ab}_q, I^a_q, $\bar{I}^{cb}_{pq}$, T^{ab}_{pq} and $\bar{O}^{ac}_{pq}$. The purpose of this article is to show that the same thing can be done with the new stable expansion. We will show that using the new expansion gives increased accuracy and stability. It also reduces the computational cost compared with the multipole expansion (§ 1 *a*).

(*b*) *Splitting the calculation along six directions*

We are going to use the two integrals in (2.1) to approximate $\mathrm{e}^{\mathrm{i}\kappa|\boldsymbol{r}_i - \boldsymbol{r}_j|}/|\boldsymbol{r}_i - \boldsymbol{r}_j|$. In order to do so, we need to satisfy the following condition.

Condition 2.3. *There must exist a constant C such that for all clusters C_a (centre $\boldsymbol{O}_a$) and C_b (centre $\boldsymbol{O}_b$) for which (2.1) is used, and for all points $\boldsymbol{r}_i = (x_i, y_i, z_i)$ and $\boldsymbol{r}_j = (x_j, y_j, z_j)$ in clusters C_a and C_b, we have*

$$\sqrt{x^2 + y^2} < C(z_j - z_i),$$

where $(x, y, z) \stackrel{\text{def}}{=} (\boldsymbol{r}_i - \boldsymbol{O}_a) - (\boldsymbol{r}_j - \boldsymbol{O}_b)$.

When this condition is satisfied, we will show that the total number of multipole terms (denoted previously by $n^{\max}$) remains small. In a standard oct-tree decomposition, if we consider two clusters in the interaction list (see Greengard & Rokhlin (1997) for a definition of the interaction list) we can always choose a set of Cartesian axes such that

$$\sqrt{x^2 + y^2} < \sqrt{2}(z_j - z_i), \quad \forall z_i \in C_a \text{ and } \forall z_j \in C_b.$$

Therefore, this condition is naturally met.

The next subsection describes the treatment of the propagative term

$$\int_{S^{z+}} \mathrm{e}^{\mathrm{i}\kappa\langle\sigma,\boldsymbol{r}\rangle}\,\mathrm{d}\sigma. \tag{2.3}$$

(c) *Propagative term*

The computation of the first integral is very close to the HF FMM. The difficulty in integrating this function is due to the discontinuity at $z = 0$, so that its Fourier spectrum decays slowly. Two strategies can be applied: one based on a spherical-harmonics decomposition and the other on Fourier decomposition. The main idea will be to remove 'high' frequencies in the transfer function $T_\sigma(\boldsymbol{r}) = \mathbf{1}_{S^{z+}}(\sigma)\mathrm{e}^{\mathrm{i}\kappa\langle\sigma,\boldsymbol{r}\rangle}$ for $\sigma \in S^2$, $\boldsymbol{r} \in \mathbb{R}^3$ in order to compute accurately the integral in (2.3).

(i) *Spherical-harmonics decomposition*

This approach is similar to HF FMM. We start by recalling the classical definition of spherical-harmonic functions.

Definition 2.4. The space of spherical harmonics is spanned by $\{Y_{lm}\}_{l\in\mathbb{N},|m|\leqslant l}$ with

$$\forall l \geqslant 0, \forall m \in \{0,\dots,l\}, \quad Y_{lm}(\sigma) = \sqrt{\frac{2l+1}{4\pi}} C_l^m P_l^m(\cos\theta)\mathrm{e}^{\mathrm{i}m\psi} \tag{2.4}$$

and

$$\forall l \geqslant 0, \forall m \in \{0,\dots,l\}, \quad Y_{l,-m} = (-1)^m Y_{l,m}^*, \tag{2.5}$$

where

$$C_l^m = \sqrt{\frac{(l-m)!}{(l+m)!}}$$

and P_l^m are the associated Legendre functions defined by

$$P_l^m(x) = (-1)^m(1-x^2)^{m/2}\frac{\mathrm{d}^m}{\mathrm{d}x^m}P_l(x); \tag{2.6}$$

$\{Y_{lm}\}_{l\in\mathbb{N},|m|\leqslant l}$ is an orthonormal basis of $L^2(S^2)$. Any function $f \in L^2(S^2)$ can be written as

$$f = \sum_{l\in\mathbb{N}}\sum_{|m|\leqslant l} \hat{f}_{lm} Y_{lm}$$

with

$$\hat{f}_{lm} = \int_{S^2} f(\sigma) Y_{lm}^*(\sigma)\,\mathrm{d}\sigma.$$

A fundamental result that we will need is that the function $\mathrm{e}^{\mathrm{i}\kappa\langle\sigma,r\rangle}$ can be approximated by a finite bandwidth function, in the following sense.

Theorem 2.5. *Let us define the function f by $f(\sigma) \stackrel{\text{def}}{=} \mathrm{e}^{\mathrm{i}\kappa\langle\sigma,\boldsymbol{r}\rangle}$. For a given $\epsilon > 0$, we have*

$$\left| f(\sigma) - \sum_{\substack{m \\ 0 \leqslant l \leqslant L}} \hat{f}_{lm} Y_{lm}(\sigma) \right| \leqslant \epsilon$$

with

$$L \approx \kappa|\boldsymbol{r}| + 1.8 d_0^{2/3} (\kappa|\boldsymbol{r}|)^{1/3} \quad \textit{and} \quad d_0 = \log(1/\epsilon).$$

Proof. The proof uses the results derived in Song & Chew (2001). ■

We now have all the elements needed to define the operators in requirement 2.2. The multipole expansion of item (1) is obtained by choosing a sufficient number of quadrature points σ_q on S^2 such that they integrate exactly all spherical harmonics up to degree $L = \kappa R + 1.8 d_0^{2/3} (\kappa R)^{1/3}$, where R is the radius of the cluster containing point $\boldsymbol{r}$. The function $I_q^a(\boldsymbol{r} - \boldsymbol{O}_a)$ is then defined as

$$I_q^a(\boldsymbol{r} - \boldsymbol{O}_a) \stackrel{\text{def}}{=} \mathrm{e}^{\mathrm{i}\kappa\langle\sigma_q, \boldsymbol{r} - \boldsymbol{O}_a\rangle}.$$

The outer-to-outer transform is a classical interpolation (see Darve 2000*a*, *b*; Chew 1993; Chew *et al*. 1994; Chew & Song 1995, 1997) followed by a multiplication by $\mathrm{e}^{\mathrm{i}\kappa\langle\sigma_q, \boldsymbol{O}_c - \boldsymbol{O}_b\rangle}$.

The outer-to-inner transform corresponds to an interpolation, a multiplication by a transfer function $T_{ab}(\sigma)$ and an anterpolation (see Darve 2000*a*, *b*). The transfer function $T_{ab}(\sigma)$ is defined in the following way. Define $T_{ab}^u(\sigma)$ by

$$T_{ab}^u(\sigma) = \begin{cases} \mathrm{e}^{\mathrm{i}\kappa\langle\sigma, \boldsymbol{O}_a - \boldsymbol{O}_b\rangle}, & \text{if } \sigma \in S^{z^+}, \\ 0, & \text{otherwise.} \end{cases}$$

Then

$$T_{ab}(\sigma) = \sum_{\substack{m \\ 0 \leqslant l \leqslant 2L}} (\widehat{T}_{ab}^u)_{lm} Y_{lm}(\sigma).$$

The truncation in spherical-harmonic space is required to reduce the number of quadrature points on S^2 to a minimum. The matrix T_{pq}^{ab} is defined as the result of the interpolation, multiplication by $T_{ab}(\sigma_q)$ and anterpolation.

The inner-to-inner transform is defined using the usual multiplication by

$$\mathrm{e}^{\mathrm{i}\kappa\langle\sigma_q, \boldsymbol{O}_a - \boldsymbol{O}_c\rangle}$$

and anterpolation (see Darve 2000*a*,*b*).

We summarize this approach in the following theorem.

Theorem 2.6. *For the propagative term, using a spherical-harmonics decomposition, the number $n^{\max}$ of sample points on S^2 needed is equal to $(L+1) \times (L+1)$, where*

$$L \approx \kappa R + 1.8 d_0^{2/3} (\kappa R)^{1/3}, \quad d_0 \stackrel{\text{def}}{=} \log(1/\epsilon),$$

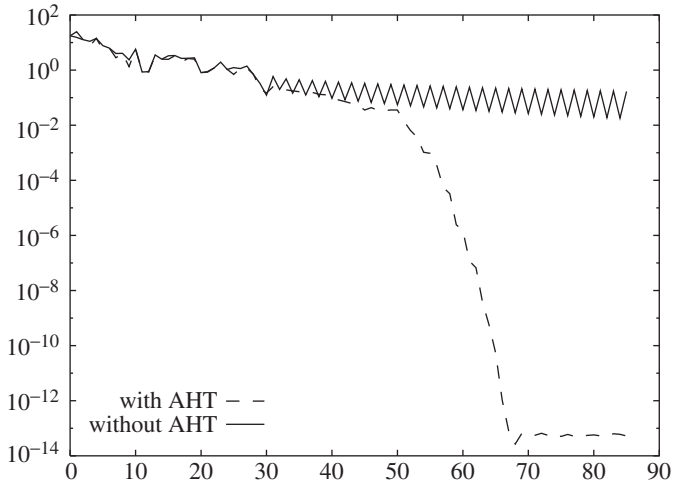

Figure 1. Accuracy of FMM when using a smoothed transfer function $T_{ab}(\sigma)$ and its non-smoothed version $T^u_{ab}(\sigma)$.

and R is the radius of the cluster. The transfer function must be chosen to be

$$T_{ab}(\sigma) \stackrel{\text{def}}{=} \sum_{\substack{m \\ 0 \leqslant l \leqslant 2L}} (\widehat{T}^u_{ab})_{lm} Y_{lm}(\sigma),$$

with

$$T^u_{ab}(\sigma) \stackrel{\text{def}}{=} \begin{cases} \mathrm{e}^{\mathrm{i}\kappa\langle\sigma, \boldsymbol{O}_a - \boldsymbol{O}_b\rangle}, & \text{if } \sigma \in S^{z^+}, \\ 0, & \text{otherwise.} \end{cases}$$

Proof. This result follows from theorem 2.5 and the fact that the spherical harmonics form an orthonormal basis of S^2. We also used the fact that

$$\exp\{\mathrm{i}\kappa\langle\sigma(\theta,\phi), \boldsymbol{r}\rangle\} = (\exp\{\mathrm{i}\kappa\langle\sigma(\pi-\theta, \pi+\phi), \boldsymbol{r}\rangle\})^*, \tag{2.7}$$

which allows the reduction, by a factor of two, of the number of discretization points along ϕ. ■

To illustrate the importance of the smoothing of $T_{ab}(\sigma)$ we performed the following test. Let us place N points in a cell of size ρ. We compare the error in the transfer step when using $T_{ab}(\sigma)$ and its non-smoothed version $T^u_{ab}(\sigma)$. The 'exact' computation is done by a very accurate integration with an error of 10^{-14}.

Figure 1 shows the error of integration for $N = 100$, $\rho = 1$, $\kappa = 10$, and a transfer vector equal to $(1, 2, 3)$.

The error by integration with the non-smoothed transfer function has a very slow decay so that a direct computation without smoothing should be really inefficient.

(ii) *Fourier decomposition*

A very similar approach can be developed using a Fourier decomposition rather than a spherical-harmonic decomposition. We follow some of the ideas of Sarvas

(2000). Let us describe a point σ in S^2 using spherical angles (θ, ϕ). The integration over ϕ is standard and can be done using the usual interpolation, smoothing of the transfer function and anterpolation. The integration over θ creates a difficulty, since apparently we are integrating only from 0 to π rather than 2π. However, this can easily be remedied by extending the domain of integration from $[0;\pi]$ to $[0;2\pi]$ and using the characteristic function $\mathbf{1}_{[0:\pi/2]}(\theta)$.

The non-smoothed transfer function can be defined as

$$T^u_{ab}(\theta,\psi) \stackrel{\text{def}}{=} \tfrac{1}{2}(\mathbf{1}_{[0:\pi/2]}(\theta)\sin\theta + \mathbf{1}_{[0:\pi/2]}(2\pi-\theta)\sin(2\pi-\theta))\mathrm{e}^{\mathrm{i}\kappa\langle\sigma(\theta,\psi),\boldsymbol{O}_a-\boldsymbol{O}_b\rangle}. \quad (2.8)$$

The first step consists of smoothing along ϕ by keeping all frequencies in Fourier space between $-2L$ and $2L$. This requires a $4L+1$ quadrature point along ϕ. The second step consists of smoothing along θ by removing all frequencies outside of $[-2L;2L]$. Note that we can choose to include the north and/or south pole. This is advantageous as for those two poles the number of points in the direction ϕ is equal to 1 rather than $4L+1$.

Using (2.8) rather than $\mathbf{1}_{[0:\pi/2]}(\theta)\sin\theta\mathrm{e}^{\mathrm{i}\kappa\langle\sigma(\theta,\psi),\boldsymbol{r}\rangle}$ allows the reduction of the storage and computational cost by two, since with (2.8) the values in the interval $[\pi;2\pi]$ are equal to the values in $[0;\pi]$.

A theorem similar to theorem 2.6 can be formulated.

Theorem 2.7. *For the propagative term, using a Fourier decomposition, the number $n^{\max}$ of sample points on S^2 needed is equal to $1+L\times(L+1)$, where*

$$L \approx \kappa R + 1.8 d_0^{2/3}(\kappa R)^{1/3}, \quad d_0 \stackrel{\text{def}}{=} \log(1/\epsilon),$$

and R is the radius of the cluster. The transfer function is obtained by smoothing the function

$$T^u_{ab}(\theta,\psi) \stackrel{\text{def}}{=} \tfrac{1}{2}(\mathbf{1}_{[0:\pi/2]}(\theta)\sin\theta + \mathbf{1}_{[0:\pi/2]}(2\pi-\theta)\sin(2\pi-\theta))\mathrm{e}^{\mathrm{i}\kappa\langle\sigma(\theta,\psi),\boldsymbol{O}_a-\boldsymbol{O}_b\rangle}.$$

Only the frequencies in Fourier space for θ and ϕ between $-2L$ and $2L$ need to be retained.

Proof. The proof is very similar to theorem 2.6. We need $2L+1$ sample points along ϕ and θ. The number of points along ϕ can be reduced to $L+1$ by using the symmetry (2.7). The number of points along θ can be reduced to $L+1$ by using the symmetry with respect to $\theta=\pi$. Finally, for the north pole, the number of points along ϕ is 1. This gives a total of $1+L(L+1)$ points. ■

In the next section we consider the second integral

$$\int_{\chi=0}^{+\infty}\int_{\phi=0}^{2\pi} \exp\{-\chi^2 z\}\exp\{\mathrm{i}\sqrt{\chi^4+\kappa^2}(x\cos\phi + y\sin\phi)\}\chi\,\mathrm{d}\chi\,\mathrm{d}\phi.$$

(*d*) *Evanescent term*

(i) *Variable ϕ*

For variable ϕ, techniques based on Fourier decomposition, similar to the ones described in § 2 *c*, can be used. The main result can be summarized by the following theorem.

Theorem 2.8. *For the propagative term, using a Fourier decomposition, the number of quadrature points needed along ϕ is equal to*

$$L_\phi \approx L_0 + 1 + 1.8 d_0^{2/3} L_0^{1/3}, \quad d_0 \stackrel{\text{def}}{=} \log(1/\epsilon),$$

with

$$L_0 \stackrel{\text{def}}{=} \frac{R_0}{\sqrt{2}} \sqrt{\left(\frac{2d_0}{R_0}\right)^2 + \kappa^2}$$

for a cluster of side length R_0.

Proof. This is a direct consequence of Song & Chew (2001). The largest value for χ^2 is $2d_0/R_0$; therefore

$$\sqrt{\chi^4 + \kappa^2}\sqrt{x^2 + y^2} \leqslant \frac{R_0}{\sqrt{2}} \sqrt{\left(\frac{2d_0}{R_0}\right)^2 + \kappa^2}.$$

In addition, the following symmetry along ϕ allows the reduction of the number of quadrature points by two:

$$\exp\{\mathrm{i}\sqrt{\chi^4 + \kappa^2}(x\cos(\pi + \phi) + y\sin(\pi + \phi))\} = (\exp\{\mathrm{i}\sqrt{\chi^4 + \kappa^2}(x\cos\phi + y\sin\phi)\})^*.$$

■

The following corollary shows that in the low-frequency regime L_ϕ is almost constant and that in the high-frequency regime it grows almost proportionally to κR_0.

Corollary 2.9. *In theorem 2.8, L_0 can be approximated by the following expressions in the low and high-frequency regime.*

(i) *When $R_0 \ll 2d_0/\kappa$, $L_0 \approx d_0\sqrt{2}$.*

(ii) *When $R_0 \gg 2d_0/\kappa$, $L_0 \approx \kappa R_0/\sqrt{2}$.*

(ii) *Variable χ*

For the variable χ we can use two approaches: one which is based on a singular value decomposition (SVD) and which we implemented, and a second one based on a Fourier decomposition. We will present partial numerical results only for the latter case. The Fourier-decomposition approach is, however, the simplest and most promising one. It will be described more completely in a future publication. Complete numerical results will be given that use the SVD.

(*e*) *SVD*

Let us consider the kernel function $K(\chi, z, \rho)$ and its integral

$$K(\chi, z, \rho) \stackrel{\text{def}}{=} \exp(-\chi z)\exp(\mathrm{i}\rho\sqrt{\chi^2 + \kappa^2}),$$
$$V(x, y, z) \stackrel{\text{def}}{=} \int_0^{+\infty} \mathrm{d}\chi \int_0^{2\pi} \mathrm{d}\phi\, K(\chi, z, x\cos\phi + y\sin\phi).$$

In order to satisfy requirement 2.2, we essentially need to define a quadrature for χ, an interpolation and anterpolation procedure. Let us see how this can be done using the SVD of K (Yarvin & Rokhlin 1996).

(i) *The SVD of a function*

Proposition 2.10. *For any $\varepsilon > 0$, there exists a set of real orthonormal functions $\{u_p(\chi)\}_{0\leqslant p<N}$, a set of complex orthonormal functions $\{v_p(z,\rho)\}_{0\leqslant p<N}$ and real positive coefficients $\{s_p\}_{0\leqslant p<N}$ such that*

$$\forall(\chi,z,\rho)\in[0:\chi_{\max}]\times[z_{\min}:z_{\max}]\times[-\rho_{\max}:+\rho_{\max}],$$
$$\left|K(\chi,z,\rho)-\sum_{p=0}^{N-1}s_p u_p(\chi)v_p(z,\rho)\right|\leqslant\varepsilon.$$

In addition $v_p(z,-\rho)=(v_p(z,\rho))^*$.

Proof. The fundamental result to prove this decomposition is the following lemma (Golub & Van Loan 1983).

Lemma 2.11 (the SVD of a matrix). *For any $n\times m$ matrix A, there exists an $n\times p$ matrix U with orthonormal columns, an $m\times p$ matrix V with orthonormal columns and a $p\times p$ real diagonal matrix $S=[s_{ij}]$ whose diagonal entries are non-negative, such that $A=USV^*$ and $s_{ii}\geqslant s_{i+1,i+1}$ for all $i=1,\dots,p-1$.*

This is useful in finite dimensions; however, K is defined on continuous ranges.

We now summarize the procedure of Yarvin & Rokhlin (1996). First, we have to discretize K on a basis which provides a finite dimension matrix. We use a basis of high-order Legendre polynomials P_l in each dimension, such that interpolation errors stay below ϵ:

$$\left|K(\chi,z,\rho)-\sum_{i,j,k}K(\chi_i,z_j,\rho_k)P_i(\chi)P_j(z)P_k(\rho)\right|\leqslant\epsilon.$$

Next, we define a matrix $A_{i,(j,k)}$, where the couple (j,k) is the column index

$$A_{i,(j,k)}=K(\chi_i,z_j,\rho_k)\sqrt{w_i^\chi w_j^z w_k^\rho}.$$

By applying the SVD to A, we obtain the factorization

$$A=USV^*,$$

where U and V are $n\times p$ and $m\times p$ matrices with orthonormal columns and S a $p\times p$ diagonal matrix.

We can then define

$$u_p(\chi)=\sum_i\frac{u_{i,p}}{\sqrt{w_p^\chi}}P_i(\chi),$$
$$v_p(z,\rho)=\sum_{j,k}\frac{u_{(j,k),p}}{\sqrt{w_j^z w_k^\rho}}P_j(z)P_k(\rho),$$

which provide orthonormal functions such that

$$\left|K(\chi,z,\rho)-\sum_{p=0}^{N-1}s_p u_p(\chi)v_p(z,\rho)\right|\leqslant\epsilon.$$

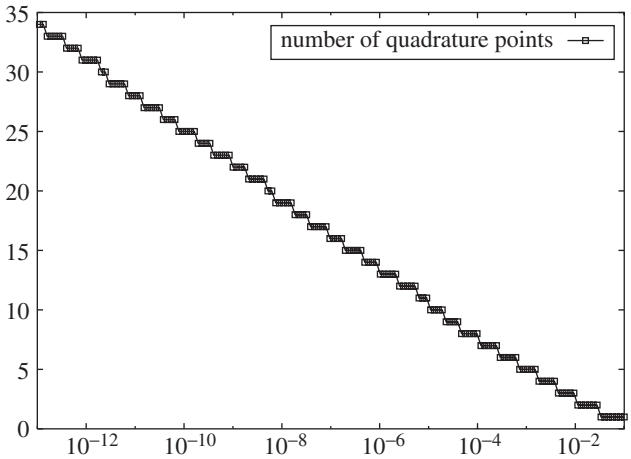

Figure 2. Number of quadrature points χ as a function of ϵ, given by SVD.

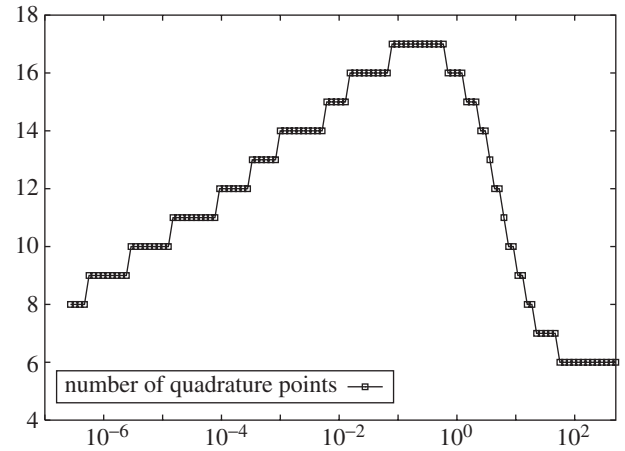

Figure 3. Number of quadrature points χ as a function of z, given by SVD.

In the special case of our kernel K, we can show that u_p is real. The following integral is real for all χ, χ':

$$\int_{z_{\min}}^{z_{\max}} \int_{-\rho_{\max}}^{\rho_{\max}} K(\chi, z, \rho)(K(\chi', z, \rho))^* \, \mathrm{d}z \, \mathrm{d}\rho.$$

Therefore, $\sum_p s_p^2 u_p(\chi)(u_p(\chi'))^*$ is real. This proves that the phase angle of $u_p(\chi)$ is independent of χ. Hence, we can always modify the phase angle of $v_p(z, \rho)$ such that $u_p(\chi)$ is real. It can then be directly shown that $v_p(z, -\rho) = (v_p(z, \rho))^*$. ■

Following the method of Yarvin & Rokhlin (1996), once $u_p(\chi)$ has been computed we can calculate N quadrature points and N weights such that they integrate exactly the first $2N$ functions $u_p(\chi)$. This yields a quadrature for

$$\int_0^{+\infty} K(\chi, z, x\cos\phi + y\sin\phi) \, \mathrm{d}\chi$$

with accuracy ϵ for all (x, y, z) such that $\sqrt{x^2 + y^2} \leqslant \rho_{\max}$ and $z \in [z_{\min} : z_{\max}]$.

Numerical tests show that a small number of terms in the SVD is sufficient for accurately approximating $K(\chi, z, \rho)$. For example, for $z = \rho = 10^{-3}$, $\kappa = 1$, we computed the number of quadrature points N as a function of the error ϵ. Figure 2 shows that N is of the order of $O(\log \epsilon^{-1})$. Figure 3 shows the dependence of N on z.

(ii) *Steps of the new FMM*

We now explain how requirement 2.2 can be satisfied. We consider only the treatment of χ, since ϕ was described earlier.

In order to simplify this presentation, we introduce some additional notation:

$$l \text{ is the level in the tree, } l = 0 \text{ at the leaf and } l = l^{\max} \text{ at the root;}$$

$$u_p^l(\chi)v_p^l(z,\rho) \text{ is the SVD decomposition at level } l \text{ in the tree;}$$

$$\boldsymbol{r} = (x, y, z) \in \mathbb{R}^3;$$

$$v_p^l(\boldsymbol{r} : \phi) \stackrel{\text{def}}{=} v_p^l(z, x\cos\phi + y\sin\phi);$$

$$K(\chi, \boldsymbol{r} : \phi) \stackrel{\text{def}}{=} K(\chi, z, x\cos\phi + y\sin\phi).$$

First we need to define the function $I_q^a(\boldsymbol{r} - \boldsymbol{O}_a)$ for the multipole expansion (item (1) in requirement 2.2):

$$I_q^a(\boldsymbol{r} - \boldsymbol{O}_a) \stackrel{\text{def}}{=} \int_0^{\chi_{\max}^l} u_q^l(\chi) K(\chi, \boldsymbol{r} - \boldsymbol{O}_a + \boldsymbol{s}_l : \phi)\,\mathrm{d}\chi, \tag{2.9}$$

where $\boldsymbol{s}_l$ is a shift vector of magnitude $\frac{3}{2}$ times the side length of the cluster and along the $+z$-direction. We need to add $\boldsymbol{s}_l$ because K is unbounded when the z-coordinate of $\boldsymbol{r} - \boldsymbol{O}_a$ is negative. This shift ensures that K remains bounded.

The outer-to-outer transform is obtained in a straightforward way by using the orthonormality of the functions $u_p^l(\chi)$. The matrix $\bar{I}_{pq}^{cb}$ can be defined as

$$\bar{I}_{pq}^{cb} \stackrel{\text{def}}{=} \int u_p^{l+1}(\chi) K(\chi, \boldsymbol{O}_c - \boldsymbol{O}_b - \boldsymbol{s}_l + \boldsymbol{s}_{l+1} : \phi) u_q^l(\chi)\,\mathrm{d}\chi.$$

Proof. This is a direct consequence of the orthonormality of $u_p^{l+1}(\chi)$ and of item 2 of requirement 2.2. ■

The outer-to-inner transform (3) is defined by the following matrix:

$$T_{pq}^{ab} = \int u_p^l(\chi) K(\chi, \boldsymbol{O}_a - \boldsymbol{O}_b - 2\boldsymbol{s}_l : \phi) u_q^l(\chi)\,\mathrm{d}\chi. \tag{2.10}$$

Again this definition results from the orthonormality of $u_p^l(\chi)$ and item (3). It is important to realize that the outer-to-inner transform can be performed efficiently if it is done in the following manner.

(i) Pre-processing step: multiply $I_q^b(\boldsymbol{O}_b - \boldsymbol{r}')$ by $u_q^l(\chi)$.

(ii) Processing step: perform all the transfers doing a simple element-by-element multiplication by $K(\chi_q, \boldsymbol{O}_a - \boldsymbol{O}_b - 2\boldsymbol{s}_l : \phi)$. This operator is diagonal (in the sense of Rokhlin (1992)).

(iii) Post-processing step: multiply by $u_p^l(\chi)$ and integrate.

The quadrature needed for the integration in (2.10) is provided by the generalized Gaussian quadrature of Yarvin (Yarvin & Rokhlin 1996).

Compared with the standard plane-wave expansion, the cost of this operation is similar.

The outer functions $O_q^{ab}(\boldsymbol{O}_a - \boldsymbol{r}')$ are now defined as

$$O_q^{ab}(\boldsymbol{O}_a - \boldsymbol{r}') \stackrel{\text{def}}{=} \int_0^{\chi_{\max}^l} u_q^l(\chi) K(\chi, \boldsymbol{O}_a - \boldsymbol{r}' - \boldsymbol{s}_l : \phi)\, \mathrm{d}\chi.$$

Using the quadrature of Yarvin & Rokhlin (1996), we now prove that the following accuracy is achievable. We will show later that this is sufficient for our purpose.

Theorem 2.12. *Consider two clusters C_a and C_b sufficiently far away. Let us consider a generalized Gaussian quadrature such that*

$$\left| \int K(\chi, \boldsymbol{r} - \boldsymbol{r}' : \phi)\, \mathrm{d}\chi - \sum_{q=1}^{N} \omega_q K(\chi_q, \boldsymbol{r} - \boldsymbol{r}' : \phi) \right| \leqslant \epsilon, \quad \forall \boldsymbol{r} \in C_a \text{ and } \forall \boldsymbol{r}' \in C_b.$$

If this quadrature is used to calculate the integral, then

$$T_{pq}^{ab} = \int u_p^l(\chi) K(\chi, \boldsymbol{O}_a - \boldsymbol{O}_b - 2\boldsymbol{s}_l : \phi) u_q^l(\chi)\, \mathrm{d}\chi.$$

Then the outer-to-inner transform allows computing $O_p^{ab}(\boldsymbol{O}_a - \boldsymbol{r}')$ with accuracy ϵ / s_p^l.

Proof. Following Yarvin & Rokhlin (1996), we can build a quadrature for χ with N points such that

$$\left| \int K(\chi, \boldsymbol{r} - \boldsymbol{r}' : \phi)\, \mathrm{d}\chi - \sum_{q=1}^{N} \omega_q K(\chi_q, \boldsymbol{r} - \boldsymbol{r}' : \phi) \right| \leqslant \epsilon.$$

The integrand can be split into

$$K(\chi, \boldsymbol{r} - \boldsymbol{r}' : \phi) = K(\chi, \boldsymbol{r} - \boldsymbol{O}_a + \boldsymbol{s}_l : \phi) K(\chi, \boldsymbol{O}_a - \boldsymbol{O}_b - 2\boldsymbol{s}_l : \phi) K(\chi, \boldsymbol{O}_b - \boldsymbol{r}' + \boldsymbol{s}_l : \phi).$$

By applying the SVD to $K(\chi, \boldsymbol{r} - \boldsymbol{O}_a + \boldsymbol{s}_l : \phi)$ and using the fact that $v_p^l(z, \rho)$ is an orthonormal basis, we have proved that our quadrature $\{(\chi_q, \omega_q)\}$ can integrate

$$s_p^l \int u_p^l(\chi) K(\chi, \boldsymbol{O}_a - \boldsymbol{O}_b - 2\boldsymbol{s}_l : \phi) K(\chi, \boldsymbol{O}_b - \boldsymbol{r}' + \boldsymbol{s}_l : \phi)\, \mathrm{d}\chi$$

with accuracy ϵ. Therefore, the error on $O_p^{ab}(\boldsymbol{O}_a - \boldsymbol{r}')$ is of the order of ϵ / s_p^l. ■

We now define the inner-to-inner transform (4).

Theorem 2.13. *For the evanescent term, using an SVD, the inner-to-inner transform is defined by the following matrix $\bar{O}_{pq}^{ac}$:*

$$\bar{O}_{pq}^{ac} \stackrel{\text{def}}{=} \int u_p^l(\chi) K(\chi, \boldsymbol{O}_a - \boldsymbol{O}_c - \boldsymbol{s}_l + \boldsymbol{s}_{l+1} : \phi) u_q^{l+1}(\chi)\, \mathrm{d}\chi,$$

$\bar{O}_{pq}^{ac}$ is the transpose of $\bar{I}_{pq}^{cb}$.

Proof. We first prove that

$$\bar{O}^{ac}_{pq} = \frac{s^{l+1}_q}{s^l_p} \int (v^l_p(z,\rho))^* v^{l+1}_q((z,\rho) + (\boldsymbol{O}_a - \boldsymbol{O}_c - \boldsymbol{s}_l + \boldsymbol{s}_{l+1} : \phi))\,\mathrm{d}z\,\mathrm{d}\rho. \tag{2.11}$$

The kernel K satisfies

$$K(\chi, \boldsymbol{r} - \boldsymbol{O}_c + \boldsymbol{s}_{l+1} : \phi) = K(\chi, \boldsymbol{r} - \boldsymbol{O}_a + \boldsymbol{s}_l : \phi) K(\chi, \boldsymbol{O}_a - \boldsymbol{O}_c - \boldsymbol{s}_l + \boldsymbol{s}_{l+1} : \phi).$$

We use the SVD decomposition to obtain

$$\begin{aligned}\sum s^{l+1}_q u^{l+1}_q(\chi) v^{l+1}_q((z,\rho) + (\boldsymbol{O}_a - \boldsymbol{O}_c - \boldsymbol{s}_l + \boldsymbol{s}_{l+1} : \phi)) \\ = K(\chi, \boldsymbol{O}_a - \boldsymbol{O}_c - \boldsymbol{s}_l + \boldsymbol{s}_{l+1} : \phi) \sum s^l_p u^l_p(\chi) v^l_p(z,\rho)\end{aligned}$$

An integration against $u^{l+1}_q(\chi)(v^l_p(z,\rho))^*$ gives (2.11).

With this identity,

$$\begin{aligned}&\sum_q \bar{O}^{ac}_{pq} O^{cb}_q(\boldsymbol{O}_c - \boldsymbol{r}') \\ &\quad = \sum_q \frac{s^{l+1}_q}{s^l_p} \int (v^l_p(z,\rho))^* v^{l+1}_q((z,\rho) + (\boldsymbol{O}_a - \boldsymbol{O}_c - \boldsymbol{s}_l + \boldsymbol{s}_{l+1} : \phi))\,\mathrm{d}z\,\mathrm{d}\rho \\ &\qquad\qquad \times \int u^{l+1}_q(\chi) K(\chi, \boldsymbol{O}_c - \boldsymbol{r}' - \boldsymbol{s}_{l+1} : \phi)\,\mathrm{d}\chi \\ &\quad = \frac{1}{s^l_p} \iint K(\chi, \boldsymbol{O}_a - \boldsymbol{r}' - \boldsymbol{s}_l : \phi)(v^l_p(z,\rho))^* K(\chi, (z,\rho))\,\mathrm{d}z\,\mathrm{d}\rho\,\mathrm{d}\chi \\ &\quad = O^{ab}_p(\boldsymbol{O}_a - \boldsymbol{r}').\end{aligned}$$

■

The last result that we need regards the accuracy of the inner-to-inner transform. This requires some analysis. Theorem 2.12 states that the coefficients $O^{ab}_q(\boldsymbol{O}_a - \boldsymbol{r}')$ are calculated with accuracy ϵ/s^l_q. This is in fact sufficient, since the final calculation is given by (2.2) and $I^a_q(\boldsymbol{r} - \boldsymbol{O}_a)$ is of the order of s^l_q (see definition 2.9). There remains to prove that the inner-to-inner transform allows calculating $O^{ab}_p(\boldsymbol{O}_a - \boldsymbol{r}')$ with accuracy ϵ/s^l_p. This is in fact true.

Proposition 2.14. *Assume that the error on $O^{cb}_q(\boldsymbol{O}_c - \boldsymbol{r}')$ is of the order of ϵ/s^{l+1}_q, then the error when calculating $O^{ab}_p(\boldsymbol{O}_a - \boldsymbol{r}')$ using the inner-to-inner transform is of the order of ϵ/s^l_p.*

This theorem is essential to ensure the accuracy of the multilevel scheme.

Proof. This is a direct consequence of (2.11). ■

(*f*) *Fourier decomposition*

We will only outline this approach since we do not yet have complete numerical results. However, since this approach is much simpler to implement than the SVD we will mention it here. This approach is based solely on Fourier decomposition

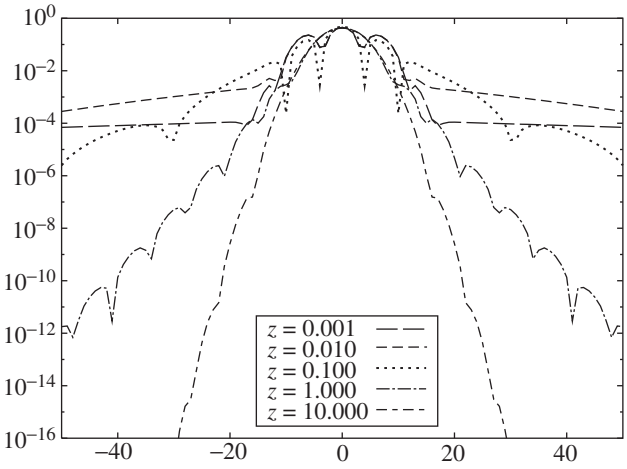

Figure 4. Spectrum of $\mathrm{Im}(K(\chi^2))$.

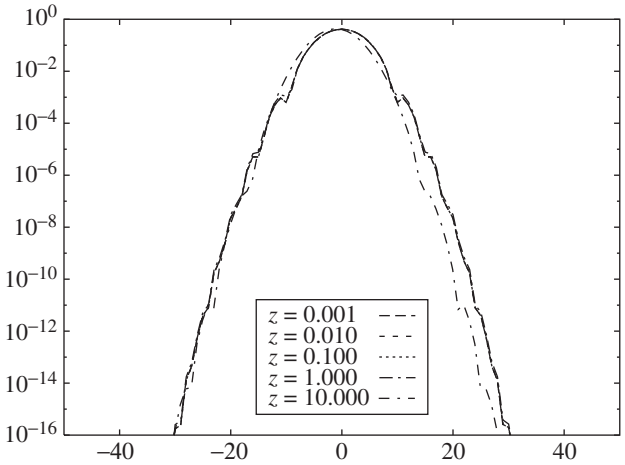

Figure 5. Spectrum of $\mathrm{Im}(K(\chi^2))/\sqrt{\chi^4+\kappa^2}$.

and therefore uses only 'classical' tools such as Fourier analysis and fast Fourier transforms.

The Fourier transform of $K(\chi^2, \boldsymbol{r} : \phi)$ has a relatively slow decay especially when $\kappa|\boldsymbol{r}| \ll 1$. However, two important facts can be observed on numerical experiments:

(i) the Fourier spectrum of $\mathrm{Re}(K(\chi^2, \boldsymbol{r} : \phi))$ decays very rapidly like a Gaussian;

(ii) the Fourier spectrum of $\mathrm{Im}(K(\chi^2, \boldsymbol{r} : \phi))/\sqrt{\chi^4+\kappa^2}$ also decays very rapidly like a Gaussian.

This is illustrated by figures 4 and 5.

Using this important result, it is possible to construct an FMM by defining all the operators of requirement 2.2. The outer-to-outer and inner-to-inner transforms are fairly straightforward and they follow the general construction of § 2 *f*. The real part $\mathrm{Re}(K(\chi^2, \boldsymbol{r} : \phi))$ is interpolated as usual. The imaginary part needs to be divided by

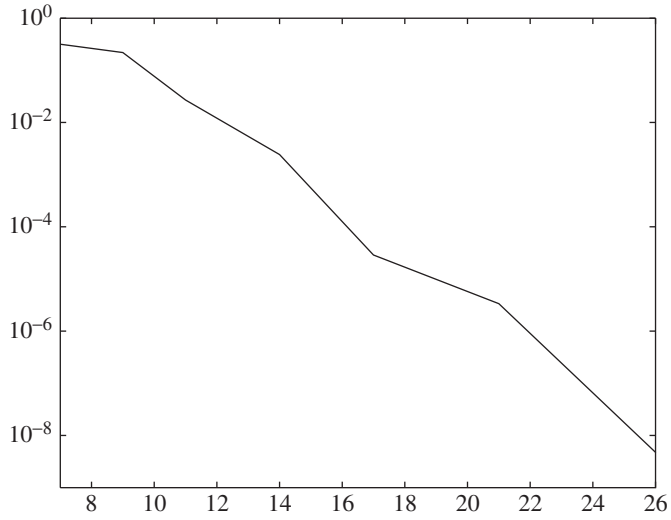

Figure 6. Error in the outer-to-outer transform with Fourier decomposition for the variable χ as a function of the number of sample points along χ.

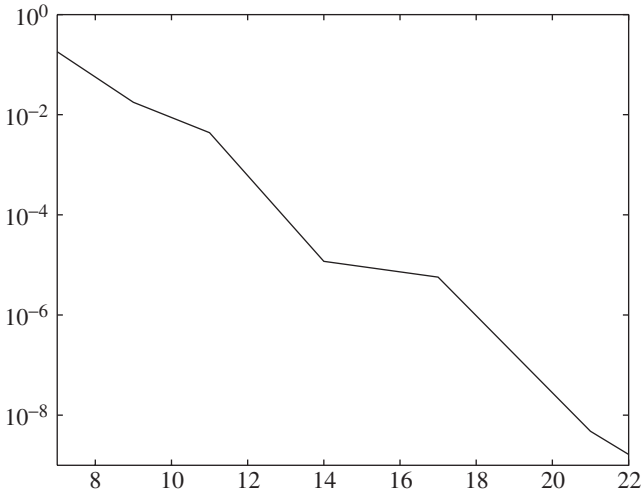

Figure 7. Error for the complete FMM with Fourier decomposition for the variable χ as a function of the number of sample points along χ.

$\sqrt{\chi^4+\kappa^2}$ then interpolated at the new sample points χ and multiplied by $\sqrt{\chi^4+\kappa^2}$. A similar operation is performed for anterpolation. Figure 6 shows the error in the outer-to-outer transform as a function of the number of sample points along χ. For this figure and for figure 7 we used eight random particles placed in two far-away clusters and $\kappa = 0.01$.

For the transfer function, we perform a smoothing as in § 2 *f*. The real part of the transfer function is smoothed as before. The imaginary part is divided by $\sqrt{\chi^4+\kappa^2}$, smoothed and then multiplied by $\sqrt{\chi^4+\kappa^2}$.

Figure 7 illustrates the decay of the error for the entire FMM (outer-to-outer, outer-to-inner and inner-to-inner transforms) for the variable χ as a function of the

Table 1. *Discretizations for* $\kappa = 0.1$, $\epsilon = 10^{-4}$

	stable plane wave		
ρ	propagative term	evanescent term	plane wave
1	3×5	$(12:4) \times 25$	—
$\frac{1}{2}$	3×5	$(12:4) \times 25$	—
$\frac{1}{4}$	3×5	$(11:4) \times 25$	—
$\frac{1}{8}$	2×3	$(11:4) \times 25$	—
$\frac{1}{16}$	2×3	$(10:3) \times 25$	—
$\frac{1}{32}$	2×3	$(10:3) \times 25$	—

Table 2. *Discretizations for* $\kappa = 1$, $\epsilon = 10^{-4}$

	stable plane wave		
ρ	propagative term	evanescent term	plane wave
1	10×20	$(5:2) \times 25$	—
$\frac{1}{2}$	8×15	$(5:2) \times 25$	—
$\frac{1}{4}$	6×12	$(5:2) \times 25$	—
$\frac{1}{8}$	5×9	$(5:2) \times 25$	—
$\frac{1}{16}$	4×8	$(5:1) \times 25$	—
$\frac{1}{32}$	3×5	$(4:1) \times 25$	—

number of sample points along χ. It was observed on numerical experiments that this error is independent of the wavenumber κ.

It is possible to reach machine precision (something not achievable with the plane-wave expansion of § 1 *b*). For example, with 30 points along χ, the error for the outer-to-outer step is 3×10^{-14} and for the complete FMM (outer-to-outer, outer-to-inner and inner-to-inner) it is 7×10^{-13}.

3. Numerical tests

(*a*) *Size of discretization*

In this section, we compare the size of the discretization for the plane-wave expansion and the stable-plane-wave expansion (tables 1–3).

The propagative term is discretized following § 2 *c* (i), which uses the same kind of operators and discretizations as the classical plane-wave expansion. For the low-frequency regime, the number of quadrature points for the propagative term goes to zero as κz goes to zero, so that its computational cost becomes negligible.

The discretization of the evanescent term is given as $(n_a : n_b) \times n_c$, which means that n_a quadrature points are used in the outer-to-inner step, n_b discretization points for the SVD, i.e. $2n_b$ functions s_p, u_p, v_p are used for the outer-to-outer

Table 3. *Discretizations for* $\kappa = 10$, $\epsilon = 10^{-4}$

	stable plane wave		
ρ	propagative term	evanescent term	plane wave
1	52×108	$(5:3) \times 83$	52×108
$\frac{1}{2}$	31×64	$(6:3) \times 49$	31×64
$\frac{1}{4}$	20×40	$(8:3) \times 33$	—
$\frac{1}{8}$	13×25	$(9:3) \times 27$	—
$\frac{1}{16}$	9×18	$(9:3) \times 25$	—
$\frac{1}{32}$	7×15	$(10:3) \times 25$	—

Table 4. *Costs of main operators:* $\kappa = 10$, $\epsilon = 10^{-4}$

ρ	HF init	PW init	HF o-to-o	PW o-to-o	HF o-to-i	PW o-to-i
1	6.80	12.38	82.40	90.8	0.691	1.056
$\frac{1}{2}$	2.40	4.56	21.05	27.0	0.244	0.503
$\frac{1}{4}$	−2.71	−10.6	−0.331			
$\frac{1}{8}$	−2.12	−5.48	−0.254			
$\frac{1}{16}$	−1.78	−2.65	−0.218			
$\frac{1}{32}$	−1.70	−2.00	−0.233			

and inner-to-inner steps, and n_c is the discretization size on ϕ. The maximal storage is $\max(n_a, 2n_b) \times n_c$.

The symbol '—' means that the value is not available because the plane-wave expansion was not stable or could not achieve the required accuracy ϵ. It is usually estimated that HF FMM becomes unstable when ρ is smaller than $\frac{1}{2}\lambda$, where $\lambda = 2\pi/\kappa$ is the wavelength.

One can notice that the stable-plane-wave expansion allows any number of levels at all frequencies.

Following theorem 2.8 and corollary 2.9, the discretization along ϕ reaches a constant size when $z \ll 1/\kappa$.

(*b*) *Computational time for each step*

Table 4 shows the cost of the main operators of the FMM algorithm (initialization of I_p^a, outer-to-outer and outer-to-inner steps) in a high-frequency regime with $\kappa = 10$ and $\epsilon = 10^{-4}$. This cost is given in seconds and corresponds to 10 000 evaluations of these operators. For this case, values for $\rho \geqslant \frac{1}{2}$ are only available for HF FMM. The stable-plane-wave expansion (PW FMM) does not follow this restriction; we can show results from $\rho = 1$ to $\rho = \frac{1}{16}$.

We see that the computational cost of I_p^a initialization (columns labelled 'init'), outer-to-outer (columns 'o-to-o') and outer-to-inner (columns 'o-to-i') steps for PW FMM in the medium to low-frequency regime, $\rho = \frac{1}{4}$ to $\rho = \frac{1}{32}$, is comparable with

Table 5. PW FMM *runtime for the cube test case:* $\kappa = 10$, $\epsilon = 10^{-4}$

	$\rho = 1$	$\rho = \frac{1}{2}$	$\rho = \frac{1}{4}$	$\rho = \frac{1}{8}$	$\rho = \frac{1}{16}$	total
propagative leaf					1.05	1.05
evanescent leaf					7.43	7.43
propagative interpolation		1.25	1.79	3.30	5.63	12.0
evanescent interpolation		0.35	1.09	3.03	6.97	11.4
propagative transfer	0.15	0.26	0.40	0.60	1.14	2.55
evanescent transfer	0.01	0.04	0.13	0.45	1.58	2.21
PW FMM						36.6
total cost including close interactions						170

Table 6. HF FMM *runtime for the cube test case:* $\kappa = 10$, $\epsilon = 10^{-4}$

	$\rho = 1$	$\rho = \frac{1}{2}$	total
leaf		11.4	11.4
interpolation		1.25	1.25
transfer	0.15	0.26	0.41
HF FMM			13.1
total cost including close interactions			1150

the cost of HF FMM at $\rho = \frac{1}{2}$. However, at $\rho = \frac{1}{2}$ and $\rho = 1$, PW FMM is computationally more expensive than HF FMM.

The next numerical test considers the total cost of the method for a model problem, a cube of size 4. We showed that the stability and accuracy of PW FMM allow an increase in the number of levels in the FMM algorithm. In the low-frequency regime, this results in a dramatic reduction in the memory and computational costs. Tables 5 and 6 show the total runtime for a cube of size 4. The unit is second. For the PW FMM case we take $\kappa = 10$, $\epsilon = 10^{-4}$ and a seven-level oct-tree. At level 1, ρ is equal to 4, and at level 7, ρ is equal to $\frac{1}{16}$. Each cell at level 7 has 100 scattering points.

Due to HF FMM restrictions, HF FMM cannot use seven levels in this example, and uses only four levels. This ensures that ρ is always larger than $\frac{1}{2}\lambda$. This restriction decreases the general performance, so that for an object scattering in the intermediate frequency regime or for large numbers of levels, PW FMM is more efficient than HF FMM.

Here are some explanations regarding tables 5 and 6.

(i) The columns 'propagative leaf' and 'evanescent leaf' show the costs of the initialization of the functions I_p^a for all the clusters at the leaf level and the final integration (2.2), respectively, for the propagative and evanescent terms. At the finest level, each box includes 100 scattering points.

(ii) The columns 'propagative interpolation' and 'evanescent interpolation' at level l show the costs of the outer-to-outer step from level l to level $2l$ and the inner-to-inner step from level $2l$ to level l for the propagative and evanescent terms.

Table 7. PW FMM *costs following the number of levels:* $\kappa = 10$, $\epsilon = 10^{-4}$

	total number of levels					
	3 levels	4 levels	5 levels	6 levels	7 levels	8 levels
propagative leaf	32.4	11.4	4.6	2.4	1.1	0.67
evanescent leaf	26.6	10.3	8.3	7.7	7.4	7.4
propagative interpolation		0.62	1.52	3.16	6.0	23.4
evanescent interpolation		0.17	0.72	2.23	5.7	38.8
propagative transfer	0.15	0.41	0.81	1.41	2.55	5.43
evanescent transfer	0.01	0.05	0.18	0.63	2.21	9.07
PW FMM	59.1	23.8	18.4	22.9	36.6	84.7
close interactions	3500	1100	300	80	20	5
total cost	3740	1200	375	170	165	345

(iii) The columns 'propagative transfer' and 'evanescent transfer' show the costs of the outer-to-inner step for the propagative and evanescent terms at each level.

(iv) Table 6 shows the same kind of results for HF FMM, which are equivalent to the propagative term in PW FMM. We are using the same number of particles for PW FMM and HF FMM. For PW FMM, since the first level is 1, we have only 100 particles per cell. On the contrary, for HF FMM, we start at level 4 and consequently we have 3000 particles per cell for the initialization step. This results in a very large computational cost for the *close interactions* step.

(v) Column *total* shows the cumulative costs for each step of the algorithm and the global costs of one iteration of the FMM algorithm at lines PW FMM and HF FMM.

This example shows that a method stable at medium and low frequencies allows the reduction of the global computational time significantly.

We made an additional test (table 7) to establish the optimal number of levels to be used. We used the same test case, a scattering cube of size 4, with the same number of particles, but with different numbers of levels from 3 to 7. The optimal number is the one that minimizes the global cost, i.e. the cost of PW FMM plus close interactions. In this case, the optimal number of levels is seven, which corresponds to about 100 particles per cluster at the leaf level.

Note that it is possible to further improve those results by using additional properties of the FMM.

4. Numerical applications

In this section, we will illustrate the stability of the method for a wide frequency range. All results are obtained by a combined-field integral-equations formulation without preconditioning. The convergence may therefore be slow, but we are only interested in the accuracy and stability of matrix–vector products with the FMM.

For these tests, we have used $\mu_0 = 1.257\,51 \times 10^{-6}$, $\epsilon_0 = 8.848\,06 \times 10^{-12}$ giving $c = 299\,792\,548.2\ \mathrm{m\ s^{-1}}$; the objects are perfectly conducting.

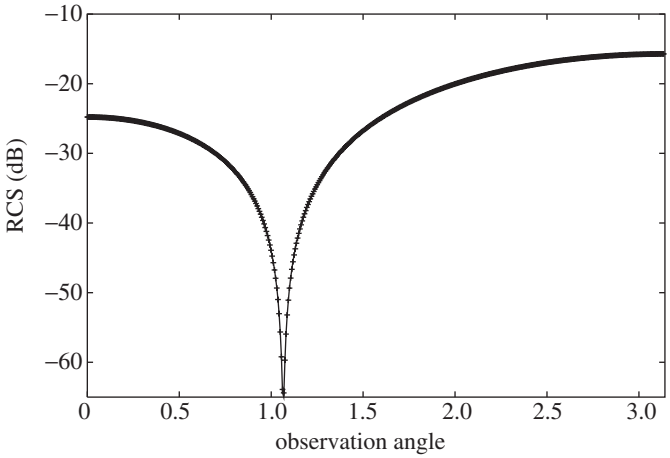

Figure 8. RCS of a unit sphere of size $\frac{1}{15}\lambda$
(+, numerical RCS; solid line, exact RCS (sphere $R = 1$)).

The targeted error is $\epsilon = 10^{-4}$ for the Kernel approximation, and the iterative solver (generalized minimal residual) stops when the residual becomes less than 10^{-4}.

These tests use a spherical-harmonic representation (§ 2 *c* (i)) for the propagative integral quadrature.

(*a*) *Low-frequency regime: sphere* $\frac{1}{15}\lambda$

This example (figure 8) shows a radar cross section (RCS) on a unit sphere of 3000 edges (degrees of freedom) with a wavelength $\lambda = 30$. The exact solution is done by Mie series.

This example has failed using the HF FMM (even level 3, the lowest level for an FMM), due to numerical instabilities on the transfer functions.

This result has been computed with 4 levels where levels from 3 to 4 are discretized with 4×6, 3×4 for propagative term and $(11 : 4) \times 28$ points at each level for the evanescent term.

(*b*) *Intermediate-frequency regime: sphere* 2λ

This example (figure 9) shows an RCS on a unit sphere of 3000 edges with a wavelength $\lambda = 1$. The exact solution is done by Mie series.

The HF FMM fails on this example when we are using more than 5 levels.

This result has been computed with 6 levels, where levels from 3 to 6 are discretized with 15×28, 10×18, 8×14, 6×10 points for the propagative term and $(9 : 3) \times 28$, $(9 : 3) \times 28$, $(10 : 3) \times 28$, $(10 : 3) \times 28$ points for the evanescent term.

(*c*) *High-frequency regime: sphere* 5.5λ

This example (figure 10) shows an RCS on a unit sphere of 18 000 edges with a wavelength $\lambda = 0.36$. The exact solution is done by Mie series.

This result has been computed with 7 levels, where levels from 3 to 7 are discretized with 28×54, 17×32, 13×24, 9×16, 7×12 points for the propagative term and

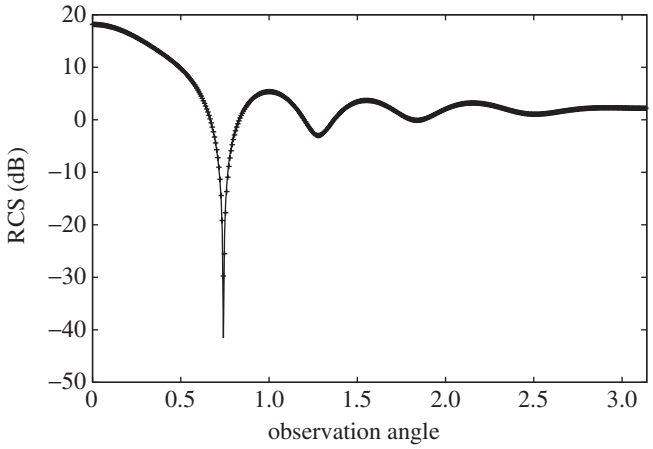

Figure 9. RCS of a unit sphere of size 2λ
(+, numerical RCS; solid line, exact RCS (sphere $R = 1$)).

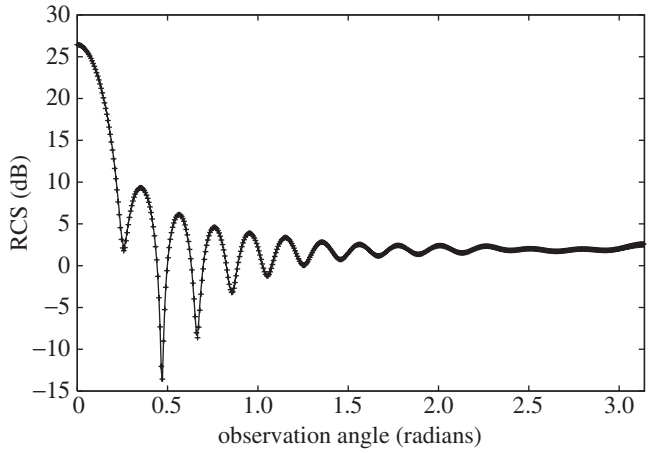

Figure 10. RCS of a unit sphere of size 5.5λ
(+, numerical RCS; solid line, exact RCS (sphere $R = 1$)).

$(7:3)\times 48$, $(8:3)\times 32$, $(9:3)\times 28$, $(9:3)\times 28$, $(9:3)\times 28$ points for the evanescent term.

(*d*) *Car* $\frac{1}{2}\lambda$

This example (figure 12) shows the electric intensity on the surface of a car of 12 000 edges. The length of the car is equal to half the wavelength of the incident wave. Figure 11 compares the FMM RCS and an accurate RCS calculated using a direct method.

The HF FMM fails on this example when we are using more than three levels.

This result has been computed with five levels, where levels from 3 to 5 are discretized with 6×10, 5×8, 4×6 points for the propagative term and $(12:4)\times 28$ points at each level for the evanescent term.

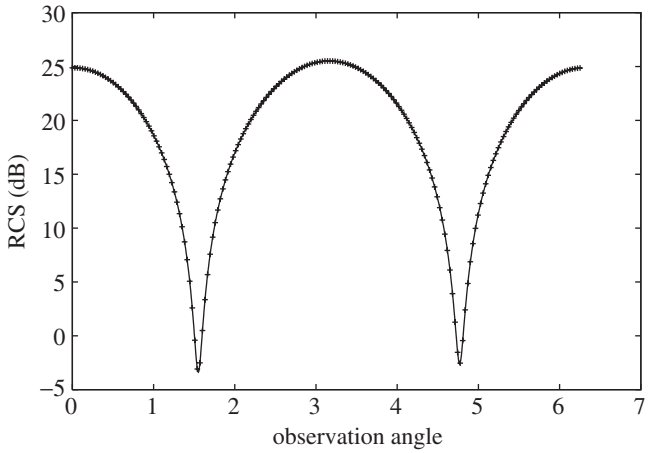

Figure 11. RCS of a car of size $\frac{1}{2}\lambda$. +, FMM RCS; solid line, accurate RCS.

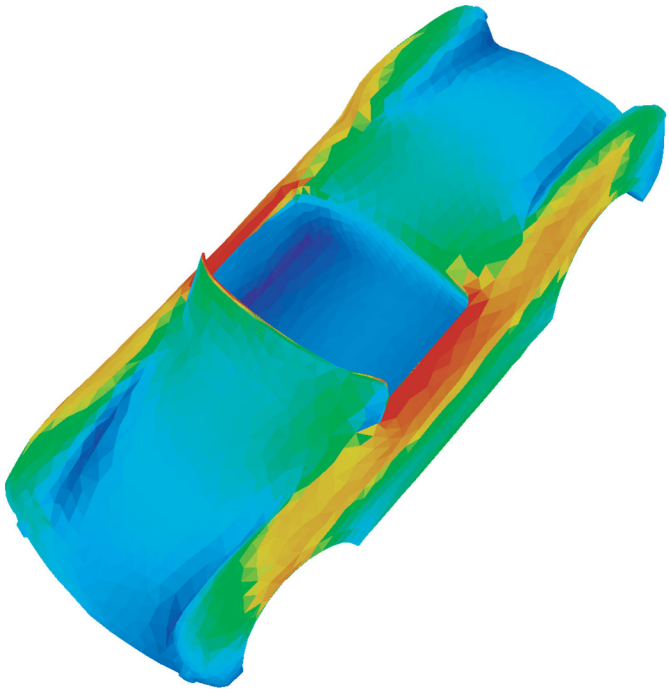

Figure 12. Electric intensity on the surface of a car.

5. Conclusion

We described a novel algorithm, the stable-plane-wave expansion, which is based on a new expansion of $\exp(\mathrm{i}\kappa r)/r$ in terms of plane waves. This new formulation of the FMM removes some restrictions of the traditional approach. In particular, it allows using clusters of an arbitrarily small size. This is advantageous for medium- to low-frequency problems, where the object is just a fraction of a wavelength long. We demonstrated on numerical examples that the computational cost in this case

is tremendously reduced compared with the traditional FMM for high-frequency applications.

Another advantage of this formulation is that it allows us to achieve any accuracy by simply increasing the number of terms in the approximation. On the contrary, the traditional FMM suffers from a numerical instability when the number of terms in the expansion is too large. Because of this, there is a lower bound on the error that can be achieved. This limitation has been removed with the stable-plane-wave expansion.

An important feature of the plane-wave expansion is that it allows us to adaptively refine the mesh with a low computational cost. This is in contrast with the traditional method for which adaptivity is costly. This is a consequence of the restriction on the size of the clusters that can be used.

We acknowledge the support of Professor Olivier Pironneau of Paris 6 University, and that of Professor Parviz Moin from Stanford University, in the accomplishment of this work and the preparation of the manuscript.

References

Chew, W. C. 1993 Fast algorithms for wave scattering developed at the University of Illinois's electromagnetics laboratory. *IEEE Antennas Propagat. Mag.* **354**, 22–32.

Chew, W. C. & Song, J. M. 1995 Multilevel fast-multipole algorithm for solving combined field integral equations of electromagnetic scattering. *Microwave Opt. Technol. Lett.* **10**, 14–19.

Chew, W. C., Lu, C.-C. & Wang, Y. M. 1994 Review of efficient computation of three-dimensional scattering of vector electromagnetic waves. *J. Opt. Soc. Am.* A **11**, 1528–1537.

Chew, W. C., Jin, J.-M., Lu, C.-C., Michielssen, E. & Song, J. M. 1997 Fast solution methods in electromagnetics. *IEEE Trans. Antennas Propagat.* **45**, 533–543.

Darve, E. 2000*a* The fast multipole method. I. Error analysis and asymptotic complexity. *SIAM J. Numer. Analysis* **38**, 98–128.

Darve, E. 2000*b* The fast multipole method: numerical implementation. *J. Computat. Phys.* **160**, 195–240.

Dembart, B. & Shubin, G. R. 1994 A 3D fast multipole method for electromagnetics with multiple levels. Technical report ISSTECH-97-004, Boeing.

Dembart, B. & Yip, E. 1994 A 3-D moment method code based on fast multipole. In *URSI Radio Sci. Meet. Digest, Seattle, WA*. p. 23.

Dembart, B. & Yip, E. 1995 A 3D fast multipole method for electromagnetics with multiple levels. In *Proc. 11th A. Rev. Progress in Applied Computational Electromagnetics, Monterey, CA*, pp. 621–628.

Elliot, W. & Board, J. 1996 Fast Fourier-transform accelerated fast multipole algorithm. *SIAM J. Sci. Comput.* **17**, 398–415.

Epton, M. A. & Dembart, B. 1995 Multipole translation theory for three-dimensional Laplace and Helmholtz equations. *SIAM J. Sci. Comput.* **16**, 865–897.

Golub, G. H. & Van Loan, C. F. 1983 *Matrix computations*. MR no 85h:65063. *Johns Hopkins Series in the Mathematical Sciences*, vol. 3, p. 476. Baltimore, MD: Johns Hopkins University Press.

Greengard, L. & Rokhlin, V. 1997 A new version of the fast multipole method for Laplace equation in three dimensions. *Acta Numerica* **229**, 229–269.

Greengard, L., Huang, J., Rokhlin, V. & Wandzura, S. 1998 Accelerating fast multipole methods for low-frequency scattering. *IEEE Comput. Sci. Engng* **5**, 32–38.

Hu, B. & Chew, W. 2000*a* Fast inhomogeneous plane wave algorithm for electromagnetic solutions in layered medium structures. *Radio Sci.* **35**, 31–43.

Hu, B. & Chew, W. 2000*b* Fast inhomogeneous plane wave algorithm for multi-layered medium problems. In *IEEE Antennas and Propagation Society Int. Symp. Transmitting Waves of Progress to the Next Millennium, Salt Lake City, UT, USA*, pp. 606–609.

Hu, B. & Chew, W. 2001 Fast inhomogeneous plane wave algorithm for scattering from objects above the multi-layered medium. *IEEE Trans. Geosci. Remote Sensing* **39**, 1028–1038.

Hu, B., Chew, W., Michielssen, E. & Zhao, J. 1999 Fast inhomogeneous plane wave algorithm for the fast analysis of two-dimensional scattering problems. *Radio Sci.* **34**, 759–772.

Hu, B., Chew, W. & Velamparambil, S. 2001 Fast inhomogeneous plane analysis of electromagnetic wave algorithm for the scattering. *Radio Sci.* **36**, 1327–1340.

Lu, C. C. & Chew, W. C. 1994 A multilevel algorithm for solving boundary-value scattering. *Microwave Opt. Technol. Lett.* **7**, 466–470.

Lu, C. C. & Chew, W. C. 1995 Fast far-field approximation for calculating the RCS of large objects. *Microwave Opt. Technol. Lett.* **8**, 1528–1537.

Rokhlin, V. 1990 Rapid solution of integral equations of scattering theory in two dimensions. *J. Computat. Phys.* **86**, 414–439.

Rokhlin, V. 1992 Diagonal forms of translation operators for Helmholtz equation in three dimensions. Research report YALEU/DCS/RR-894, Department of Computer Science, Yale University, USA.

Sarvas, J. 2000 Performing interpolation and anterpolation entirely by fast Fourier transform in the 3-D multilevel fast multipole algorithm. Research report no. CCEM-13-00, Center for Computational Electromagnetics and Electromagnetics Laboratory, University of Illinois at Urbana-Champaign, IL, USA.

Song, J. M. & Chew, W. C. 2001 Error analysis for the truncation of multipole expansion of vector Green's functions. *IEEE Microw. Wireless Compon. Lett.* **11**, 311–313.

Song, J., Lu, C. C. & Chew, W. 1997 Multilevel fast multipole algorithm for electromagnetic scattering by large complex objects. *IEEE Trans. Antennas Propagat.* **45**, 1488–1493.

Song, J., Lu, C. C., Chew, W. & Lee, S. 1998*a* Fast Illinois solver code (FISC). *IEEE Trans. Antennas Propagat.* **40**, 27–33.

Song, J., Lu, C. C., Chew, W. & Lee, S. 1998*b* Fast Illinois solver code (FISC) solves problems of unprecedented size at the Center For Computational Electromagnetics. Technical report CCEM-23–97, University of Illinois, USA.

Velamparambil, S. & Chew, W. C. 2001 Fast polynomial representation for the translation operators of an MLFMA. *Microwave Opt. Technol. Lett.* **28**, 298–303.

Wagner, R. L. & Chew, W. C. 1994 A ray-propagation fast multipole algorithm. *Microwave Opt. Technol. Lett.* **7**, 435–438.

White, C. & Headgordon, M. 1996 Rotating around the quartic angular-momentum barrier in fast multipole method calculations. *J. Chem. Phys.* **105**, 5061–5067.

Yarvin, N. & Rokhlin, V. 1996 Generalized Gaussian quadratures and singular value decompositions of integral operators. Report no. 1109, Department of Computer Science, Yale University, USA.

Zhao, J.-S. & Chew, W. 1999 MLFMA for solving integral equations of 2-D electromagnetic problems from static to electrodynamic. *Microwave Opt. Technol. Lett.* **20**, 306–311.

Zhao, J.-S. & Chew, W. 2000*a* Three-dimensional multilevel fast multipole algorithm from static to electrodynamic. *Microwave Opt. Technol. Lett.* **26**, 43–48.

Zhao, J.-S. & Chew, W. 2000*b* Applying matrix rotation to three-dimensional low-frequency multilevel fast multipole algorithm. *Microwave Opt. Technol. Lett.* **26**, 105–110.

Zhao, J.-S. & Chew, W. 2001 Applying LF-MLFMA to solve complex PEC structures. *Microwave Opt. Technol. Lett.* **28**, 155–160.

Zhao, J.-S., Chew, W. C., Cui, T. & Zhang, Y. 2002 Cancellations of surface loop basis functions. In *IEEE Antennas and Propagation Society Int. Symp., 16–21 June 2002, San Antonio, TX, USA*, vol. 1, pp. 58–61.